A COMPREHENSIVE ASSESSMENT OF X-/GAMMA RAY ATTENUATION CHARACTERISTICS OF SELECTED RAW MATERIALS COMMONLY USED IN DENTAL APPLICATIONS

A. M. Osman

Physics Department, College of Science, Jouf University, Sakaka, P.O.Box 2014, Saudi Arabia

Email: ***amoa@ju.edu.sa***

ABSTRACT

The application of dental X-ray imaging and gamma-ray sterilization is a base to the diagnosis and assessment of a wide range of oral and maxillofacial conditions. In this study, the interaction mechanisms of X-/gamma-ray photons with nine commonly used dental restorative and treatment materials were systematically evaluated. To accomplish this, several key radiation-attenuation parameters, including the mass and linear attenuation coefficients (μ_m, μ), mean free path (MFP), atomic and electronic cross sections ($\sigma_{t.a}$, $\sigma_{t.el}$), effective electron density (N_{eff}), as well as the equivalent and effective atomic numbers (Z_{eq}, Z_{eff}) were calculated and analyzed over a broad photon-energy range (15 keV to 15 MeV). The computations were performed using the EpiXS software package, and the obtained results were further verified through comparison with data generated by the NIST-XCOM database. A detailed investigation was carried out at twelve discrete characteristic X-ray energy levels between 0.008 and 0.05 MeV. In addition, mass attenuation coefficients (μ_m) were calculated for γ-ray emissions from widely used radionuclides, including ^{241}Am, ^{133}Ba, ^{109}Cd, ^{152}Eu, ^{57}Co, ^{60}Co, ^{137}Cs, ^{22}Na, ^{152}Eu, ^{54}Mn, ^{55}Fe, and ^{131}I. Given that the principal aim of this investigation was to evaluate the X-/γ-ray shielding capabilities of the tested dental materials, their corresponding shielding metrics particularly buildup factors (BUFs) were also analyzed using the GP-fitting interpolation method. Furthermore, the attenuation behavior of these materials was systematically compared with several reference shielding materials documented in the literatures. The linear attenuation coefficient of all investigated samples reduced quickly with the increase in energy, at the beginning, while decrease more slowly in the region from ~ 270 keV to ~ 850 keV. The effective atomic number of high-noble alloy and noble alloy are comparatively higher than the Z_{eff} of the remaining samples, while acrylic possesses the lowest effective atomic number. The half value layer results showed that high-noble alloy (highest density) is more effective to attenuate the X-/γ-ray photons. On the other hand, high-noble alloy had the lowest BUFs in both lower (0.015–0.08 MeV) and higher (5–15 MeV) energy regions. The findings reveal that the high-noble alloy exhibits the greatest attenuation capability among all investigated samples. Overall, this study offers detailed insight into how common dental restorative materials interact with ionizing radiation, providing valuable guidance for enhancing patient safety and strengthening diagnostic accuracy in dental radiographic practices.

ABSTRAK

Penggunaan pengimejan sinar-X pergigian dan pensterilan sinar gamma adalah asas kepada diagnosis dan penilaian pelbagai keadaan mulut dan maksilofasial. Dalam kajian ini, mekanisme interaksi foton

sinar-X/gamma dengan sembilan bahan pemulihan dan rawatan pergigian yang biasa digunakan telah dinilai secara sistematik. Untuk mencapai matlamat ini, beberapa parameter pengecilan sinaran utama, termasuk pekali pengecilan jisim dan linear (μ_m, μ), min laluan bebas (MFP), keratan rentas atom dan elektronik (σ_t.a, σ_t.el), ketumpatan elektron berkesan (Neff, dan telaga Z sebagai setara dengan julat lebihan kavalen foton-5 ke kavalen lebar foton-15. MeV). Pengiraan telah dilakukan menggunakan pakej perisian EpiXS, dan keputusan yang diperolehi selanjutnya disahkan melalui perbandingan dengan data yang dijana oleh pangkalan data NIST-XCOM Satu penyiasatan terperinci telah dijalankan pada dua belas tahap tenaga sinar-X ciri diskret antara 0.008 dan 0.05 MeV Di samping itu, pekali pengecilan jisim digunakan secara meluas ($\mu m\gamma$) untuk pekali pengecilan radio. 241Am, 133Ba, 109Cd, 152Eu, 57Co, 60Co, 137Cs, 22Na, 531Fen Memandangkan matlamat utama penyiasatan ini adalah untuk menilai keupayaan perisai sinar-X bagi bahan pembina pergigian yang diuji juga adalah perisai metrik BUF yang sepadan dengannya. Kaedah interpolasi pemasangan GP Selanjutnya, kelakuan pengecilan bahan-bahan ini secara sistematik dibandingkan dengan beberapa bahan pelindung rujukan yang didokumenkan dalam literatur Pekali pengecilan linear bagi semua sampel yang disiasat berkurangan dengan cepat dengan peningkatan tenaga, pada mulanya, sementara berkurangan dengan lebih perlahan di kawasan daripada ~ 270 keV no aloi adalah lebih tinggi berbanding Zeff bagi sampel yang selebihnya, manakala akrilik mempunyai nombor atom berkesan terendah Hasil lapisan nilai separuh menunjukkan bahawa aloi mulia tinggi (ketumpatan tertinggi) adalah lebih berkesan untuk melemahkan foton sinar-X Sebaliknya, aloi mulia tinggi mempunyai BUF yang paling rendah dalam kedua-dua kawasan MeV1 yang lebih rendah (0.085–5 bahawa aloi bermutu tinggi mempamerkan keupayaan pengecilan yang paling besar di antara semua sampel yang disiasat Secara keseluruhannya, kajian ini menawarkan pandangan terperinci tentang cara bahan pemulihan pergigian biasa berinteraksi dengan sinaran mengion, memberikan panduan berharga untuk meningkatkan keselamatan pesakit dan mengukuhkan ketepatan diagnostik dalam amalan radiografi pergigian.

Keywords: Dental materials, Characteristic X-ray, Absorption coefficients, Build-up factors, EpiXS, XCOM approaches.

INTRODUCTION

The use of radioactive sources is increasing in various fields, including medicine, agriculture, industry, space exploration, and power generation. This use has led to increased human exposure to different types of ionizing radiation, which may have a harmful effect on the biological system [1-5]. Climate change also has led to the use of nuclear power plants as distinct sources of energy. However, these stations emit a variety of dangerous ionizing radiation. Despite concerns raised by nuclear accidents around the world such as Three Mile Island and Chernobyl, the rate of power generation using nuclear plants has been increasing over the past 60 years. [6].

It is necessary to use effective and proper shielding materials for each type of ionizing radiation. Therefore, it is necessary to use appropriate shielding not only to mitigate the harmful biological effects of radiation but also to ensure effective management of radioactive waste. In this context, many materials have been studied to select low-density structural materials to reduce energy consumption, operating expenses and radiation-hazards [7, 8]. These materials which have the distinctive properties of high density, melting point and mechanical strength, as well as high corrosion resistance and low cost, are particularly important in the design of shielding against ionizing

radiation. Lead, is the traditional and most effective absorber of photons [X-rays or gamma rays] due to its high density and atomic number [Z], but it has limitations such as high toxicity, poor mechanical strength and low melting point. These factors make its use alone insufficient in various radiation protection applications [9, 10]. Furthermore, lead shields shows limited absorption capacity for photons with low energy [in the energy range of 40–88 keV], referred to as the weak lead absorption region [11]. Many studies, including those related to various ceramic materials [12–15], polymer composites [16–19], glass systems [20–22], metal alloys [23–27], and hydride and borohydride metals [28] have been conducted in search of effective materials that can replace conventional shielding facilities provided by lead-based materials and various types of concrete.

In the present study, the photon attenuation characteristics of several raw materials commonly employed in dental restorative and therapeutic applications were systematically evaluated. The interaction properties of X-/γ-ray photons were quantified using two well-established deterministic computational tools: EpiXS [29] and NIST-XCOM [30]. Attenuation parameters were computed across a broad energy range (15 keV–15 MeV), encompassing diagnostic, therapeutic, and environmental radiation levels. The calculated shielding quantities included the mass attenuation coefficient (μ_m), effective atomic number (Z_{eff}), effective electron density (N_{eff}), as well as the atomic and electronic cross sections ($\sigma_{t.a}$ and $\sigma_{t.el}$). Furthermore, the derived attenuation parameters were benchmarked against those of conventional shielding materials reported in the literature to assess the comparative protective potential of the tested dental materials.

MATERIALS AND METHOD OF COMPUTATION

In the present work, nine dental restorative and treatment materials were selected for evaluation of their X-/γ-ray shielding capabilities. The elemental compositions and corresponding densities for each material were obtained from [31]. Table 1 summarizes the material categories, classifications, densities, and chemical compositions expressed as weight fractions. Additionally, Fig. 1 illustrates the density (g/cm^3), atomic density (atoms/b · cm), and mean atomic number (Z_{ave}) for the investigated samples. The radiation shielding performance of the selected samples was evaluated using the EpiXS code, with results cross-validated against NIST XCOM data. EpiXS computes attenuation coefficients for materials over the photon energy range, based on the EPICS2017 electron-photon interaction library [29]. In parallel, XCOM provides photon attenuation coefficients for elements, mixtures, and compounds across the same energy domain using the Berger–Hubbell database [30].

Table 1. Types, chemical compositions and classes of dental materials.

Sample	Element	Atom Fraction	Weight Fraction	Mean Atomic Number [Z_{ave}]	Density [g/cm^3]	Atom Density x 10^{-2} [atoms/b-cm]
Acrylic	H	53.588	8.1492	3.600013	1.104	9.96107
	C	33.442	60.6016			
	N	0.19609	0.4144			
	O	12.7739	30.8348			
Composite	Al	11.900	7.00	20.74641	1.930	2.54
	Si	71.800	44.0			
	Ba	16.300	49.0			
Biomimetic filler [Hydroxyapatite Ca5[PO4]3OH]	H	4.5463	0.2007	11.363478	3.160	8.33466
	O	59.090	41.407			
	P	13.636	18.4987			
	Ca	22.726	39.8936			

Oxides [Zirconium]	O	66.327	25.8617	18.650386	6.800	9.97983
	Al	0.4024	0.264626			
	Y	1.6355	3.54348			
	Zr	31.635	70.3302			
Amalgam [low copper]	Cu	8.3023	5.00	45.703488	9.190	5.24507
	Zn	3.2279	2.00			
	Ag	63.582	65.0			
	Sn	24.888	28.0			
Amalgam [High copper]	Cu	42.942	30.5	39.368635	9.340	6.28684
	Zn	1.3685	1.00			
	Pd	0.8407	1.00			
	Ag	43.544	52.5			
	Sn	11.305	15.0			
Base alloy [Nickel base]	Pd	58.756	58.0	46.630388	10.90	6.08905
	Ag	33.979	34.0			
	Sn	7.265	8.00			
High-Noble alloy [Au-Ag-Pt]	Ag	30.373	19.3	69.20063	18.40	6.5275
	Pt	8.052	9.20			
	Au	61.622	71.5			
Noble alloy [Au-Cu-Ag-Pd-III]	Cu	19.682	10.95	48.784380	12.400	6.53771
	Zn	3.756	2.15			
	Pd	4.669	4.35			
	Ag	53.104	50.15			
	Au	18.789	32.4			

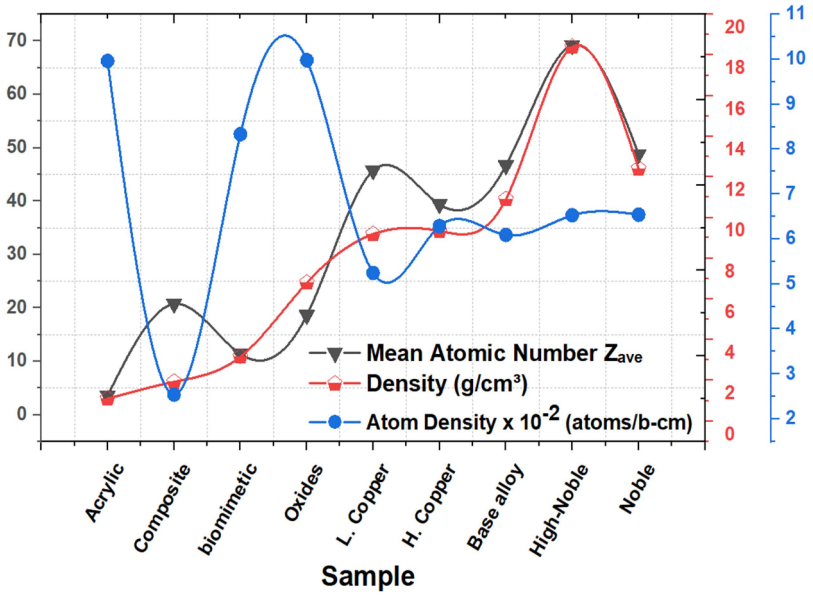

Fig 1. Properties of the investigated dental materials.

THEORETICAL BACKGROUND

The linear attenuation coefficient [μ, cm^{-1}] is a parameter that describes the fraction of incident photons in a mono-energetic beam per unit thickness of a material. It can be evaluated using the following relation:

$$\boldsymbol{\mu = \frac{1}{X} ln \frac{I_0}{I}} \quad [1]$$

Where I_0 and I are the original intensity and intensity at a thickness of x cm. Similarly, mass attenuation coefficient [μ_m, cm^2/g] is the normalization of μ per unit density of the tested material as [32, 33]:

$$\boldsymbol{\mu_m = \frac{\mu}{\rho}} \quad [2]$$

For a mixture/composited, μ_m can be evaluated by [34]:

$$\boldsymbol{\mu_m = \sum_i w_i [\mu_m]_i} \quad [3]$$

Where w_i is the weight fraction of the i^{th} constituent in the tested samples.

The half-value layer [HVL] and mean free path [MFP] are the alternate parameters for examined the shielding abilities of materials. The minimum HVL and MFP values are required for radiation shielding design and can be evaluated using [35, 36]:

$$\boldsymbol{HVL = \frac{ln[2]}{\mu}} \quad [4]$$

$$\boldsymbol{\text{MFP [cm]} = \frac{1}{\mu}} \quad [5]$$

Atomic cross-section [σ_a, cm^2/g] and electronic cross-section [σ_e, cm^2/g] are the total cross-section areas that an atom and electron of the examined material provide for interaction with photons, respectively. σ_a and σ_e are given by the following relations:

$$\boldsymbol{\sigma_a [cm^2/g] = [\mu_m] \frac{\sum_i n_i A_i}{N_A \sum_i n_i}} \quad [6]$$

$$\boldsymbol{\sigma_e [cm^2/g] = \frac{\sum_i f_i A_i [\mu_m]_i / Z_i}{N_A}} \quad [7]$$

Where N_A, A_i, n_i, f_i, and Z_i indicate the Avogadro's number, mass number, number of atoms, fractional abundance, and the atomic number of i^{th} component of a mixture/compound, respectively [37].

The effective atomic number [Z_{eff}] and effective electron density [N_{eff}] are very important parameters when it comes to choosing a proper material for radiation shielding and detection. The Z_{eff} and N_{eff} values of investigated dental samples are given by [33]:

$$\boldsymbol{Z_{eff} = \frac{\sum_i f_i A_i [\mu_m]_i}{\sum_j f_j A_j [\mu_m]_j} = \frac{\sigma_a}{\sigma_e}} \quad [8]$$

$$\boldsymbol{N_{eff} = \frac{\mu_m}{\sigma_e}} \quad [9]$$

Where μ_m, σ_e, and σ_a indicated the total mass attenuation coefficient, electronic and atomic cross sections, respectively.

In the actual shielding design, analysis of γ-photons attenuation from an extended source of radiation can be estimated by multiplying the un-collided point kernel by the buildup factor [BUF]. BUF is divided into two types; exposure buildup factor [EBF] and energy absorption buildup factor [EABF]. The calculation procedures of EBF and EABF are the same except for the coefficients used available in ANSI database. The Geometric Progression [G-P] fitting is a method used to calculate the BUF and explained in detail elsewhere [38, 39].

RESULTS AND DISCUSSION

The calculated results of mass attenuation coefficients (μ_m, $cm^2.g^{-1}$) for the analyzed dental materials are presented in Table 2. These values were obtained using the EpiXS code and independently verified with NIST-XCOM. The relative deviations between the two datasets are also provided in this table. As indicated, the μ_m values produced by EpiXS show excellent agreement with those from NIST-XCOM, with discrepancies varies from 0.017 % to 0.2921 %. Overall, High-Noble, Noble, and Base alloys exhibit the greatest attenuation coefficients across most photon energies, whereas Acrylic, Composite, and biomimetic filler materials consistently show the lowest and nearly comparable μ_m values.

A detailed evaluation was performed across twelve characteristic X-ray energies ranging from 0.008 to 0.05 MeV. In addition, mass attenuation coefficients (μ_m) were calculated for γ-ray emissions from several widely used radioisotopes, including ^{241}Am, ^{133}Ba, ^{109}Cd, ^{152}Eu, ^{57}Co, ^{60}Co, ^{137}Cs, ^{22}Na, ^{54}Mn, ^{55}Fe, and ^{131}I. The corresponding data are summarized in Table 3. The results illustrate a pronounced dependence of μ_m on photon energy. As shown, the mass attenuation coefficients for all investigated dental materials decline rapidly at low photon energies, primarily due to the strong energy dependence of the photoelectric absorption process. At intermediate energies, approximately between 0.284 MeV (^{131}I) and 0.835 MeV (^{54}Mn), the rate of decrease becomes more gradual, reflecting the dominant contribution of the Compton scattering mechanism in this region [26].

The computed linear attenuation coefficients (μ, cm^{-1}) for commonly used dental materials are illustrated in Fig. 2. As shown from this figure, μ decreases sharply as photon energy increases, primarily due to the rapid decline of the photoelectric absorption cross section with energy. At low photon energies, the curves exhibit a more gradual decline between approximately 300 and 800 keV, where Compton scattering becomes the dominant interaction mechanism. Below 300 keV, the differences in μ among the studied materials are more pronounced and diminish steadily as photon energy rises. In this lower energy region, μ is influenced by both atomic number and material density, resulting in greater variation among samples. Conversely, at high photon energies, μ becomes largely independent of atomic number, and the materials exhibit nearly identical attenuation behavior. For instance, the difference between μ for High-Noble alloy and Acrylic at 1500 keV is only 0.00516, corresponding to 9.24 %. Overall, the figure shows that the High-Noble alloy consistently exhibits the highest μ values, indicating superior photon attenuation capability relative to the other examined dental materials.

Figure 3 presents a comparison of the linear attenuation coefficients (μ) of the High-Noble alloy with those of widely used shielding materials and selected alloys, including ordinary concrete (OC), limestone concrete [40], and two low-density high-entropy alloys designated HEA6 and HEA9 [41]. Overall, the results demonstrate that the High-Noble alloy exhibits substantially higher μ values than all other materials considered. For example, at a photon energy of 20 keV, the μ values (cm^{-1}) for High-Noble alloy, ordinary concrete, limestone concrete, HEA6, and HEA9 are 1229.2, 17.7883, 29.7508, 51.8581, and 54.7893, respectively.

Figure 4 illustrates the variation of μ across photon energies emitted from common radioactive sources such as ^{241}Am, ^{133}Ba, ^{109}Cd, ^{152}Eu, ^{60}Co, ^{137}Cs, ^{22}Na, and ^{131}I. The highest attenuation occurs at 26.34 keV, corresponding to the emission from ^{241}Am. At this energy, the μ values (cm^{-1}) are 0.39496, 15.1234, 9.52366, 177.656, 342.331, 316.325, 504.925, 752.878, and 525.92 for Acrylic, Composite, Biomimetic filler, Oxides, low-Copper alloy, high-Copper alloy, Base alloy, High-Noble alloy, and Noble alloy, respectively. Additionally, noticeable discontinuities appear in the attenuation curves for Oxides, low-Copper, high-Copper, Base alloy,

High-Noble, and Noble alloy. These sharp changes correspond to the X-ray K-absorption edges of high-Z constituent elements, Ag (25.5 keV), Sn (29.2 keV), Pd (24.3 keV), Pt (78.39 keV), and Au (80.72 keV). By contrast, such distinct absorption edges are absent in the remaining materials, as the edges of their constituent elements are relatively small or lie outside the investigated energy range.

Table 2. Computed mass attenuation coefficients [cm^2/g] using EPiXS and XCOM codes for the selected dental materials.

Energy [MeV]	Acrylic			Composite			biomimetic filler		
	EpiXS	XCOM	Δ_1	EpiXS	XCOM	Δ_2	EpiXS	XCOM	Δ_3
0.001	2768.32	2769	-0.00025	4986.96	4959	-0.00564	4194.32	4196	0.0004
0.002	399.537	399.7	-0.00041	2514.61	2516	5.52E-04	662.159	662.7	0.000816
0.004	51.9255	51.91	0.000299	431.776	432.5	0.00167	183.574	184.1	0.00286
0.008	6.42481	6.423	0.000282	195.043	195.4	0.00183	87.9502	87.86	-0.00103
0.010	3.32393	3.321	0.000881	108.059	107.9	-0.00147	47.2523	47.2	-0.00111
0.020	0.56828	0.5673	0.001725	16.5835	16.6	9.94E-04	6.57248	6.56	-1.90E-03
0.040	0.23487	0.2347	0.000724	12.3451	12.39	0.00362	0.99049	0.9877	-0.00282
0.080	0.17515	0.1752	-0.00029	2.06336	2.054	-0.00456	0.2595	0.2589	-0.00232
0.100	0.16414	0.1642	-0.00037	1.17387	1.168	-0.00503	0.20221	0.2019	-0.00154
0.200	0.13291	0.1329	7.52E-05	0.26382	0.2629	-0.0035	0.12971	0.1297	-7.71E-05
0.400	0.10312	0.1032	-0.00078	0.11075	0.1108	4.51E-04	0.09629	0.09633	4.15E-04
0.800	0.07642	0.07647	-0.00065	0.06888	0.069	0.00174	0.07072	0.07077	7.07E-04
1.000	0.06868	0.06876	-0.00116	0.06061	0.0607	0.00181	0.06349	0.06356	0.0011
2.000	0.04792	0.048	-0.00167	0.04264	0.0427	0.00187	0.04468	0.04475	0.00156
4.000	0.03281	0.03289	-0.00244	0.03399	0.0340	0.00206	0.0323	0.03237	0.00216
8.000	0.02312	0.02318	-0.0026	0.03182	0.0318	0.00157	0.02566	0.02571	0.00194
10.000	0.021	0.02105	-0.00238	0.03221	0.0322	0.00155	0.02453	0.02458	0.00203
12.000	0.01956	0.01961	-0.00256	0.03287	0.0329	0.00122	0.02389	0.02394	0.00209
14.000	0.01854	0.01859	-0.0027	0.03361	0.0336	0.00119	0.02354	0.02358	0.0017
15.000	0.01814	0.01819	-0.00276	0.03398	0.0340	0.00147	0.02343	0.02347	0.0017
Average	0.001764			0.00017			0.000434		
Energy [MeV]	Oxides			Amalgam [low copper]			Amalgam [High copper]		
	EpiXS	XCOM	Δ_4	EpiXS	XCOM	Δ_5	EpiXS	XCOM	Δ_6
0.001	4287.12	4288	2.05E-04	7423.61	7417	-8.91E-04	8224.26	8223	-1.53E-04
0.002	780.141	782.9	0.00352	1530.57	1532	9.33E-04	1677.76	1679	7.39E-04
0.004	651.865	651.4	-7.14E-04	1131.57	1136	0.0039	944.376	948.1	0.00393
0.008	102.998	103	1.94E-05	214.532	214.5	-1.49E-04	169.682	169.8	6.95E-04
0.010	56.1324	56.21	0.00138	131.808	131.7	-8.20E-04	152.615	152.7	5.57E-04
0.020	53.6383	53.57	-0.00127	20.2596	20.37	0.00542	23.6293	23.71	0.0034
0.040	8.4793	8.454	-0.00299	16.9824	16.97	-7.31E-04	13.6577	13.64	-0.0013
0.080	1.31653	1.311	-0.00422	2.63465	2.626	-0.00329	2.11896	2.112	-0.0033
0.100	0.75445	0.7518	-0.00352	1.46207	1.458	-0.00279	1.18523	1.182	-0.00273
0.200	0.19762	0.1972	-0.00213	0.29614	0.2955	-0.00217	0.25747	0.2569	-0.00222
0.400	0.10014	0.1002	5.99E-04	0.11242	0.1125	7.11E-04	0.10742	0.1075	7.44E-04

0.800	0.06695	0.06704	0.00134	0.06712	0.06727	0.00223	0.06686	0.067	0.00209
1.000	0.05947	0.05956	0.00151	0.05874	0.05886	0.00204	0.05885	0.05896	0.00187
2.000	0.04219	0.04228	0.00213	0.04173	0.04182	0.00215	0.04184	0.04193	0.00215
4.000	0.03352	0.03359	0.00208	0.03567	0.03574	0.00196	0.03501	0.03508	0.002
8.000	0.03128	0.03132	0.00128	0.03674	0.03679	0.00136	0.03513	0.03519	0.00171
10.000	0.03165	0.0317	0.00158	0.03828	0.03833	0.0013	0.03634	0.03639	0.00137
12.000	0.03227	0.03231	0.00124	0.03988	0.03993	0.00125	0.03764	0.03769	0.00133
14.000	0.03295	0.03299	0.00121	0.04141	0.04146	0.00121	0.03893	0.03897	0.00103
15.000	0.0333	0.03334	0.0012	0.04213	0.04217	9.49E-04	0.03954	0.03958	0.00101
Average	0.00085			0.000729			0.000746		
Energy [MeV]	Oxides			Amalgam [low copper]			Amalgam [High copper]		
	EpiXS	XCOM	Δ_7	EpiXS	XCOM	Δ_8	EpiXS	XCOM	Δ_9
0.001	6838.9	6837	-2.78E-04	5089.74	5093	6.40E-04	6511.4	6512	9.21E-05
0.002	1357.16	1359	0.00135	1176.71	1182	0.00448	1410.79	1414	0.00227
0.004	1223.8	1230	0.00504	1170.49	1171	4.36E-04	1121.78	1125	0.00286
0.008	210.7	210.6	-4.75E-04	207.649	208.2	0.00265	191.216	191.4	9.61E-04
0.010	116.05	116	-4.31E-04	117.099	117.9	0.00679	131.244	131.6	0.00271
0.020	17.7057	17.84	0.00753	66.8045	66.86	8.30E-04	39.8984	39.98	0.00204
0.040	16.7893	16.76	-0.00175	13.7366	13.75	9.75E-04	14.1923	14.18	-8.67E-04
0.080	2.59002	2.582	-0.00311	2.80078	2.877	0.02649	2.21772	2.247	0.01303
0.100	1.43646	1.432	-0.00311	4.42895	4.431	4.63E-04	2.53041	2.529	-5.58E-04
0.200	0.29161	0.2911	-0.00175	0.79966	0.7981	-0.00195	0.48144	0.4805	-0.00196
0.400	0.11158	0.1117	0.00107	0.19701	0.1972	9.63E-04	0.14439	0.1445	7.61E-04
0.800	0.06689	0.06702	0.00194	0.08215	0.08235	0.00243	0.07321	0.07337	0.00218
1.000	0.05857	0.0587	0.00221	0.06723	0.06745	0.00326	0.06234	0.0625	0.00256
2.000	0.04164	0.04174	0.0024	0.04482	0.04496	0.00311	0.04313	0.04324	0.00254
4.000	0.03564	0.03571	0.00196	0.04046	0.04054	0.00197	0.03741	0.03748	0.00187
8.000	0.03676	0.03681	0.00136	0.04448	0.04453	0.00112	0.03926	0.03931	0.00127
10.000	0.03832	0.03837	0.0013	0.04715	0.0472	0.00106	0.04112	0.04117	0.00121
12.000	0.03994	0.03998	0.001	0.04975	0.04979	8.03E-04	0.043	0.04304	9.29E-04
14.000	0.04148	0.04152	9.63E-04	0.0522	0.05225	9.57E-04	0.04479	0.04484	0.00112
15.000	0.0422	0.04224	9.47E-04	0.05333	0.05338	9.37E-04	0.04563	0.04568	0.00109
Average	0.000908			0.002921			0.001805		

Table 3. Computed mass attenuation coefficients [μ_m, cm^2/g] of selected dental materials for photons energies emitted from radioactive sources and characteristic X-rays.

Characteristic X-ray [NIST-XCOM]										
E [MeV]	Source	Acrylic	Composite	Filler	Oxides	Low-copper	High-copper	Base-alloy	High-Noble	Noble-alloy
0.008	Cu-29	7.085	279.400	113.100	123.70	214.000	182.800	205.100	199.300	194.000
0.009		5.170	212.800	85.080	93.270	162.200	138.500	155.300	152.700	147.900
0.013	Rb-37	1.535	71.580	26.910	30.200	57.380	64.240	51.160	129.200	95.350
0.015		1.117	52.770	19.420	22.050	42.100	47.120	37.500	146.500	100.600
0.017	Mo-42	0.746	34.700	12.470	17.970	27.550	30.870	24.500	98.800	67.470

0.020		0.561	25.080	8.830	70.440	19.840	22.250	17.630	72.810	49.510
0.022	Ag-47	0.435	18.050	6.248	51.770	14.240	15.980	12.650	53.240	36.090
0.025		0.349	12.960	4.413	37.750	10.200	11.950	35.560	38.810	27.860
0.032	Ba-56	0.246	6.440	2.134	19.070	30.780	26.590	29.690	22.790	24.780
0.036		0.219	4.537	1.498	13.480	21.960	18.950	21.160	16.230	17.650
0.044	Tb-65	0.192	15.130	0.877	7.732	12.700	10.960	12.260	9.452	10.270
0.050		0.181	10.920	0.645	5.465	9.061	7.806	8.735	6.756	7.323

Radioactive Isotopes [EPiXS]

E [MeV]	Source	Acrylic	Composite	Filler	Oxides	Low-copper	High-copper	Base-alloy	High-Noble	Noble-alloy
0.014	Am [241]	1.364	45.350	18.940	23.182	55.436	64.693	48.554	149.821	95.916
0.103		0.163	1.092	0.197	0.704	1.355	1.100	1.331	4.114	2.350
0.031	Ba [133]	0.295	5.124	1.959	17.180	33.661	27.227	33.448	27.251	28.256
0.384		0.105	0.115	0.098	0.103	0.117	0.111	0.116	0.211	0.152
0.023	Cd [109]	0.438	11.206	4.365	36.947	13.641	15.891	11.883	46.027	27.272
0.088		0.170	1.617	0.231	1.032	2.042	1.647	2.007	6.103	3.497
0.014	Co [57]	1.221	40.385	16.773	20.606	49.381	57.650	43.246	153.412	93.462
0.136		0.150	0.563	0.159	0.379	0.673	0.558	0.662	2.025	1.165
1.173	Co [60]	0.063	0.055	0.059	0.055	0.054	0.054	0.053	0.059	0.056
1.332		0.059	0.052	0.055	0.051	0.050	0.050	0.050	0.054	0.052
2.506		0.042	0.039	0.040	0.039	0.039	0.039	0.039	0.042	0.040
0.284	Cs [137]	0.117	0.158	0.111	0.132	0.167	0.153	0.165	0.371	0.243
0.662		0.083	0.077	0.077	0.074	0.076	0.075	0.075	0.100	0.085
0.040	Eu [152]	0.237	12.730	1.020	8.760	17.531	14.101	17.334	14.176	14.650
1.528		0.055	0.048	0.051	0.048	0.047	0.047	0.047	0.050	0.048
0.006	Fe [55]	16.360	384.999	202.215	235.26	478.998	380.465	471.768	451.143	423.119
0.007		11.938	330.701	152.846	177.74	365.304	289.748	359.483	346.957	323.611
0.284	I [131]	0.117	0.157	0.111	0.131	0.167	0.153	0.165	0.369	0.242
0.723		0.080	0.073	0.074	0.071	0.071	0.071	0.071	0.091	0.079
0.835	Mn [54]	0.075	0.067	0.069	0.065	0.065	0.065	0.065	0.079	0.071
0.511	Na [22]	0.093	0.092	0.087	0.086	0.091	0.089	0.091	0.137	0.109
1.275		0.061	0.053	0.056	0.052	0.051	0.051	0.051	0.056	0.053

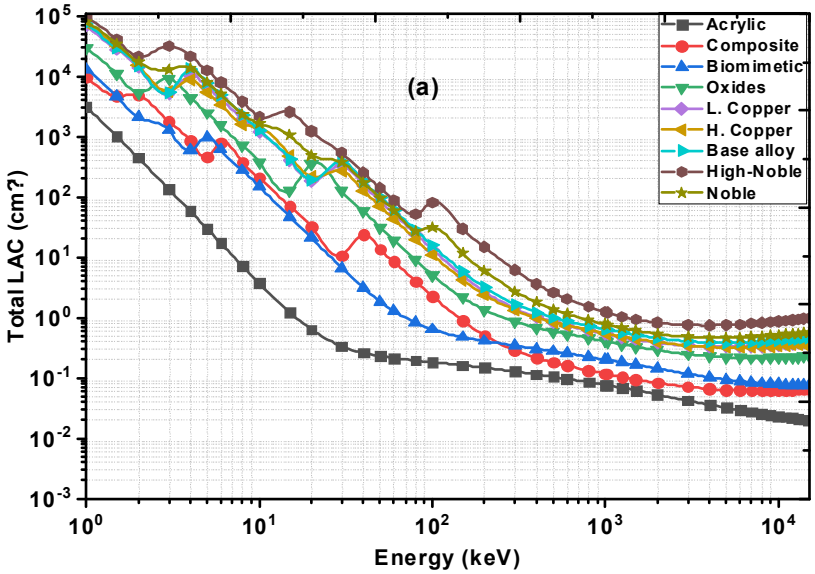

Fig 2. Variations of μ [cm^{-1}] as a function of photon-energy for the selected dental materials.

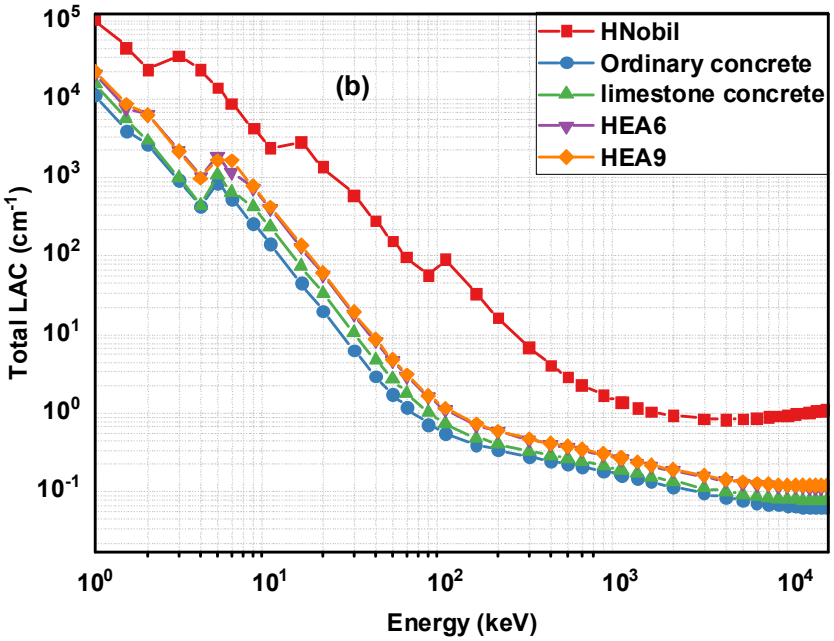

Fig 3. Variations of μ as a function of photon-energy for High-Noble alloy and other comparable conventional materials.

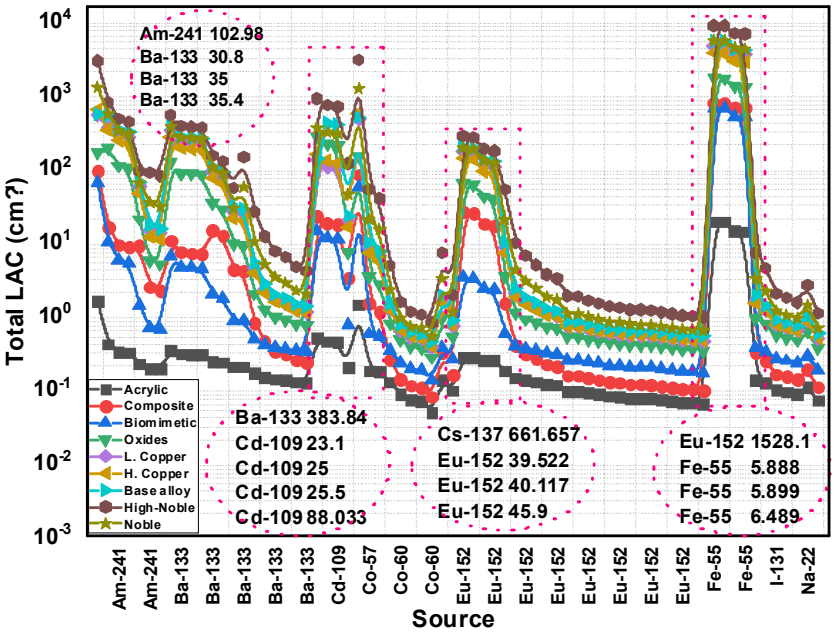

Fig 4. Variations of computed μ as a function of various photon energies emitted from different common sources for the selected dental materials.

The half-value layer (HVL) and mean free path (MFP) are key indicators of a material's radiation-shielding efficiency. HVL represents the thickness required to reduce the incident photon intensity by half, making it a practical parameter for determining the material thickness needed to achieve adequate attenuation. MFP, defined as the average distance traveled by a photon before undergoing an interaction, describes the rate at which radiation loses energy within the shielding medium. The trends of HVL and MFP with photon energy are illustrated in Figs. 5 and 6, respectively. Both quantities exhibit an inverse relationship with the linear attenuation coefficient (μ), and thus depend strongly on material density. Consequently, High-Noble alloy having the highest density among the studied samples shows the lowest HVL and MFP, indicating superior shielding performance, while low-density materials such as acrylic display the highest values. The displayed figures further demonstrate that HVL and MFP remain relatively small at lower photon energies (below a few hundred keV) but increase substantially with energy due to the dominance of Compton scattering up to approximately 8 MeV, followed by a slight decline at higher energies as pair production becomes significant. Detailed evaluations of the dental materials against standard shielding media were displayed in Figs. 5b and 6b. These figures illustrate the half-value layer (HVL) and mean free path (MFP) values for the High-Noble alloy in comparison with ordinary concrete, limestone concrete, and two low-density high-entropy alloys (HEA6 and HEA9). The High-Noble alloy consistently shows the lowest HVL and MFP values across the entire examined photon energy range compared with the other evaluated materials. This significant difference clearly indicates its superior shielding capability when compared with commonly used shielding materials.

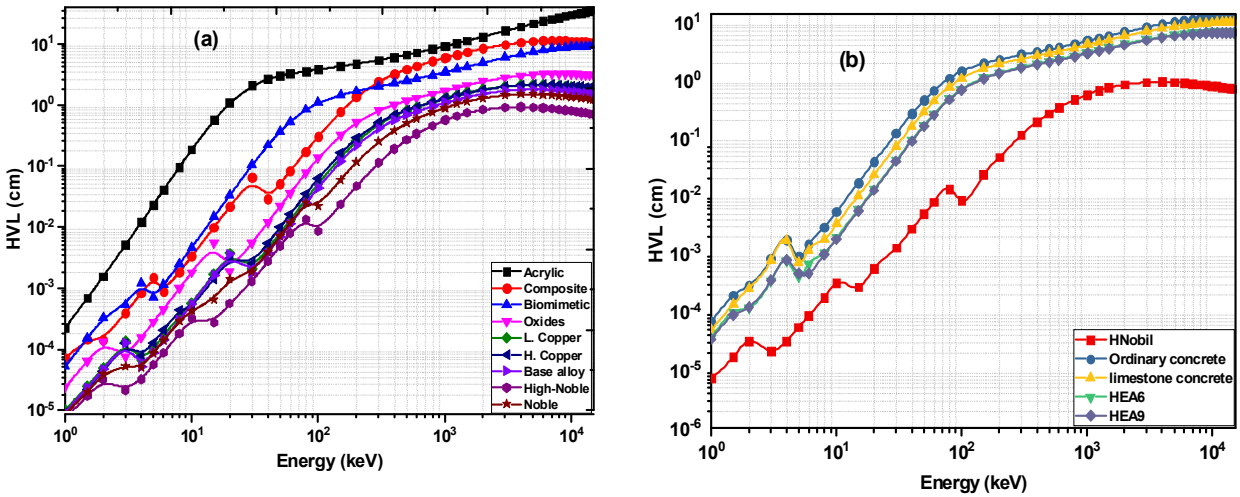

Figs 5. Behavior of [a] HVL as a function of photon-energy, and [b] comparison of HVL with different conventional materials.

The total cross-sectional area that an atom and an electron of a material have to interact with photons is known as the atomic cross section [$\sigma_{t.a}$] and the electron cross section [$\sigma_{t.el}$], respectively. $\sigma_{t.a}$ and $\sigma_{t.el}$ give the exact probability of photon interactions per atom or electron per unit volume of the shielding material. [42]. Higher values of $\sigma_{t.a}$ and $\sigma_{t.el}$ result in better shielding due to the increased probability of collision between photons and atoms. Figs. 7(a, b) show the variation of $\sigma_{t.a}$ and $\sigma_{t.el}$ with photon energy. It can be seen from these figures that $\sigma_{t.a}$ and $\sigma_{t.el}$ follow a similar trend with energy, both decreasing as energy increases. A noticeable difference between $\sigma_{t.a}$ and $\sigma_{t.el}$ can be seen from the enlarged section of the figure in the photon energy region 0.5–4 MeV, where $\sigma_{t.el}$ and $\sigma_{t.a}$ vary within the tested samples. Both quantities are higher for H-Noble, Noble, and Base alloys but lowest for Acrylic in overall energy values.

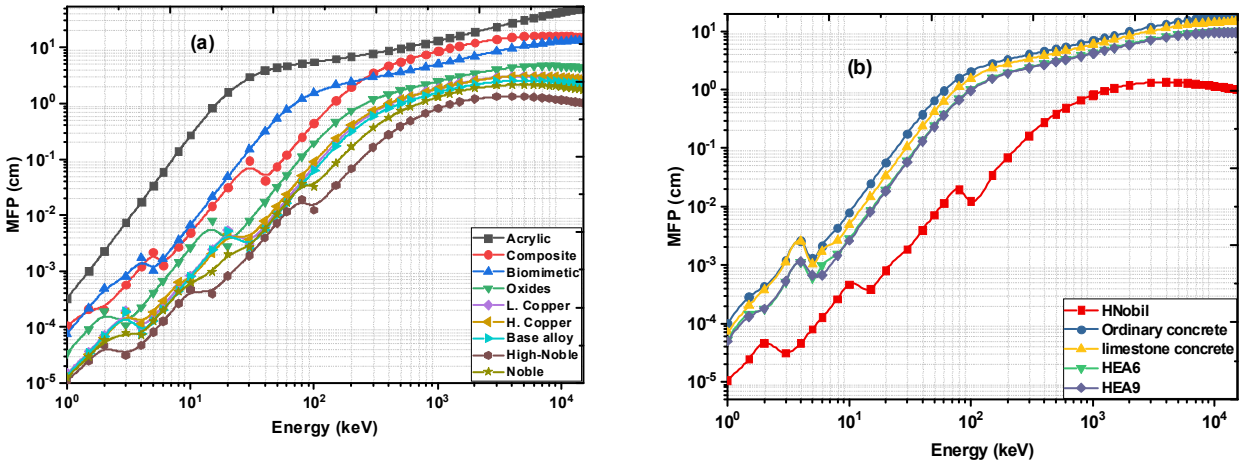

Figs 6. Behavior of [a] MFP as a function of photon-energy, and [b] comparison of MFP with different conventional materials.

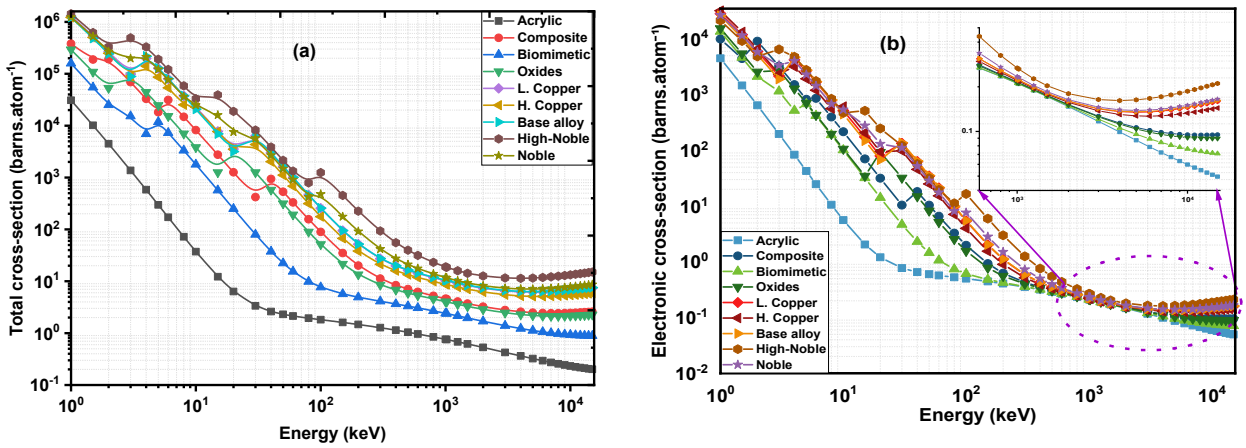

Figs 7. Behaviors of [a] $\sigma_{t.a}$, and [b] $\sigma_{t.el}$ as a function of the photon-energy.

Effective atomic number (Z_{eff}) is a key parameter that represents the effective nuclear charge of a material and is calculated using the expression: $\boldsymbol{Z_{eff} = \sigma_a \sigma_e^{-1}}$, where σ_a and σ_e denote the atomic and electronic cross sections, respectively [33]. Materials with higher Z_{eff} values generally provide superior radiation shielding [6]. In the current study, Z_{eff} was determined using two approaches. The first is an interpolation method, in which Z_{eff} is calculated for both partial and total photon interaction processes. The second is a direct method that evaluates Z_{eff} only for total photon interactions. The obtained results from these two methods for the selected dental materials are presented in Figs. 8 (a–b). As shown, the variation in Z_{eff} is governed by the dominant photon interaction mechanism at each energy region. At low photon energies, where the photoelectric effect predominates, the distribution of Z_{eff} reflects the photoelectric absorption behavior. The values of Z_{eff} increase slightly up to approximately 15 keV, reach a maximum within the 15–60 keV range, and then decrease rapidly. Between 0.2 and 2 MeV, Z_{eff} remains nearly constant due to the increasing influence of coherent and incoherent scattering processes. Above 2 MeV, Z_{eff} gradually increases again as incoherent scattering and pair production become more significant. The displayed figures further show distinct peaks at the low energy region. These peaks are due to different X-ray absorption edges of constituent elements, as discussed above. Overall, High-Noble, Noble, and base alloys exhibit the highest Z_{eff} values across the full energy range. Figure 8(c) illustrates the relative differences (δ%) between the two calculation methods. The results show strong agreement in the energy region from 0.1 MeV to 10 MeV, where Compton scattering dominates. However, notable discrepancies emerge at lower energies (10–50 keV) and at energies above 10 MeV. Additionally, Fig. 8(d) presents the average differences (δ_{avg}), which range from 0.035 to 15.8 across the entire energy spectrum.

Distribution of the electron densities [N_{eff}, electrons/g] with the incident photon energy was displayed in Figs. 9 [a-c]. The observed behaviors are almost similar to the trends shown in Figs. 8 [a-c] for Z_{eff}; where the distribution can be explained on the similar basis as discussed above. The average differences [δ_{avg}] between the two different methods ranging from 0.035 to 30.3 in the overall energy region are displayed in Fig. 9 [d].

Beyond the previously discussed parameters, two additional factors are essential for evaluating photon shielding under broad-beam conditions: the exposure buildup factor (EBF) and the energy-absorption buildup factor (EABF). A buildup factor represents the ratio of scattered radiation to uncollided radiation at a given location. The theoretical basis for calculating these quantities was introduced by Harima [38]. To determine EBF and EABF, the equivalent atomic number (Zeq) of each material is first calculated using the logarithmic interpolation method:

$$\boldsymbol{Z_{eq} = \frac{Z_1(logR_2 - logR) + Z_2[logR - logR_1]}{[logR_2 - logR_1]}}$$

The ANSI/ANS-6.4.3 reference library provides Z_{eq} values and geometric-progression (G-P) fitting parameters for elements with Z = 4 to 40, allowing interpolation of Zeq for the dental materials under study. The computed

R and Zeq values as a function of photon energy are shown in Figs. 10 and 11. These results indicate that high-noble, noble, and base alloys generally exhibit the highest Zeq and lowest R values, signifying superior shielding capabilities compared to the other materials. Next, five G-P fitting parameters (a, b, c, d, and X_k) for each material are derived using the same interpolation method. Table 3 presents the calculated Z_eq and G-P parameters for acrylic and high-noble alloy as examples. Using these parameters, EBF and EABF values are computed for photon energies from 0.015 to 15 MeV and penetration depths ranging from 1 to 40 mean free paths (MFP). The resulting buildup factors at selected photon energies are illustrated in Figs. 12 (a–d).

The behavior of EBF and EABF can be interpreted in relation to three main factors: (a) the photon energy (E), (b) the penetration depth, and (c) the chemical composition of the materials under investigation. Figures 13(a–d) illustrate the trends in EBF and EABF for acrylic; worst sample and for the high-noble alloy, which demonstrates the best performance. As shown, EBF and EABF values are minimal at low photon energies, rise significantly as the energy increases, and subsequently decrease at higher energy levels.

Unlike photoelectric absorption at low energies and pair production at high energies, photons are fully absorbed in those respective regions. In the intermediate energy range, the increased buildup factors (BUFs) are mainly due to Compton scattering, which lowers the photon's energy instead of completely absorbing it [43]. This scattering process generates additional secondary photons that increase the probability of interactions within the material, thereby raising both EBF and EABF values [42]. The sudden increases in BUFs seen in Figs. 13(b) and 13(d) at approximately 25.5, 78.39, and 80.72 keV correspond to the K-absorption edges of Ag, Pt, and Au, respectively. At these energies, the Compton scattering cross section scales with Z^{4-5} for high-Z elements. Overall, the EABF values generally exceed the EBF values across most photon energies, indicating that materials with higher Zeq tend to absorb more energy in air than within the material matrix [33].

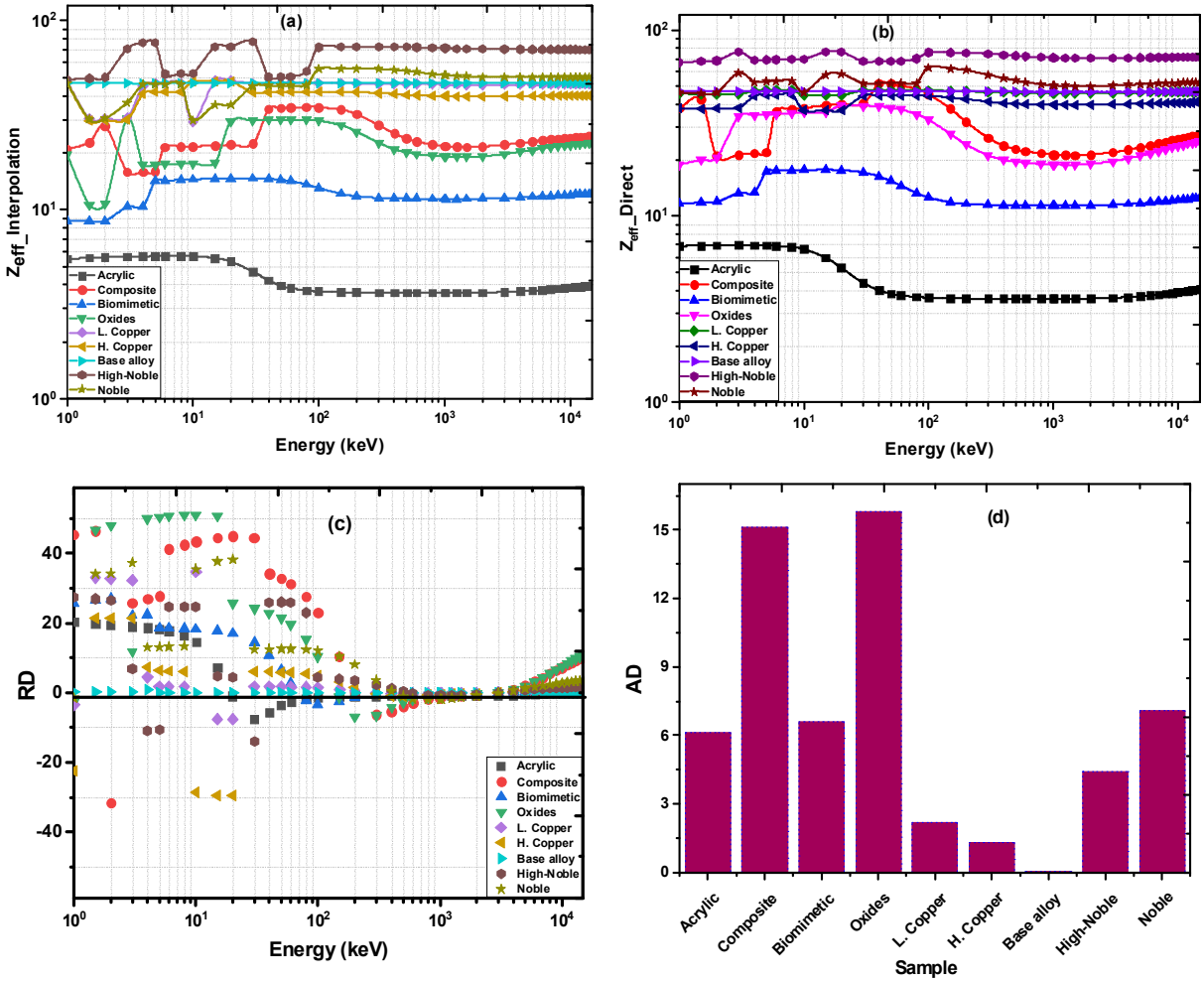

Fig 8. Effective atomic number [Z_{eff}] computed with the two different methods versus photon energy for some commonly used dental materials, [**a**] Interpolation method, [**b**] Direct method, [**c**] Relative differences [RD] between the two methods, and [**d**] Average differences [AD] between the two methods.

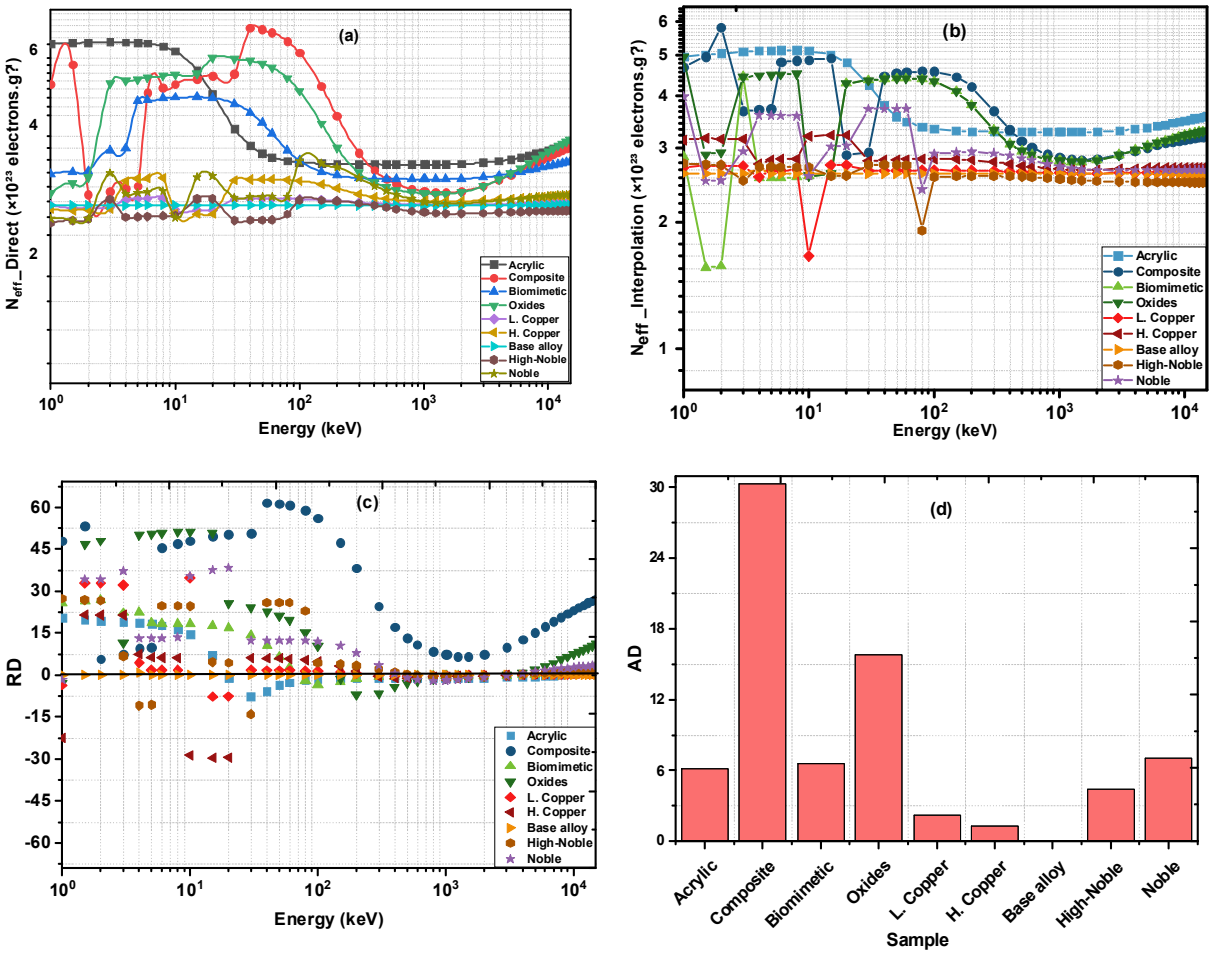

Fig 9. Effective electron densities [N_{eff}] computed with the two different methods versus photon energy for some commonly used dental materials, [**a**] Interpolation method, [**b**] Direct method, [**c**] Relative differences [δ %] between the two methods, and [**d**] Average differences [$\delta_{avg.}$] between the two methods.

Figures 14(a–d) illustrate the variation of EBF and EABF with incident photon energy at fixed penetration depths of 4 MFP and 40 MFP. These results show that both EBF and EABF increase proportionally with penetration depth and are strongly influenced by the chemical composition of the materials, particularly their effective atomic number (Z_{eff}). From the presented analysis, high-noble alloy consistently exhibits the lowest EBF and EABF values in the energy range from 0.15 MeV to 5 MeV, making it the most effective shielding material, whereas acrylic shows the highest values and therefore the poorest shielding performance. In this energy interval, the minimum EBF and EABF values achieved by the high-noble alloy were 1.25 and 1.59, respectively. Noble and base alloys also display relatively low EBF and EABF values in this region, indicating their suitability for γ-ray attenuation. However, as shown in Figures 14(a–d), high-noble, noble, and base alloys exhibit the highest buildup factors at elevated photon energies (6–15 MeV), making them less desirable as shielding materials in this high-energy range.

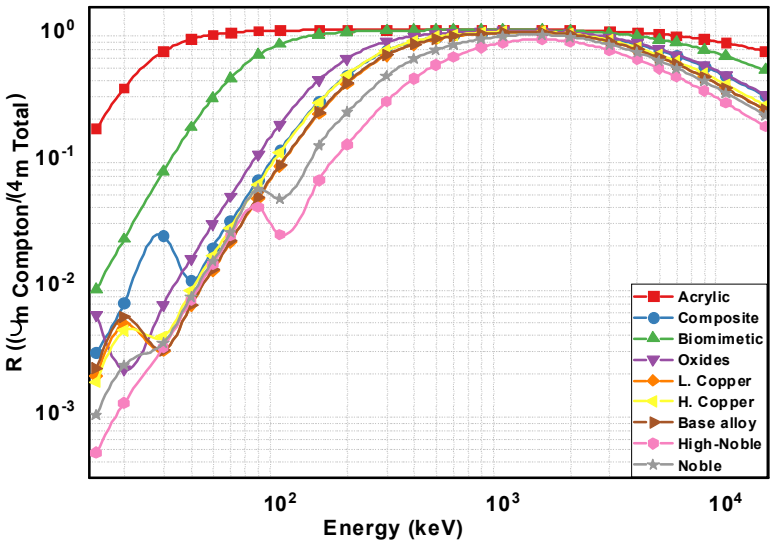

Fig 10. The variation of $\boldsymbol{R} = [\mu_m]_{Compton}/[\mu_m]_{Total}$ with the energy for the selected dental samples.

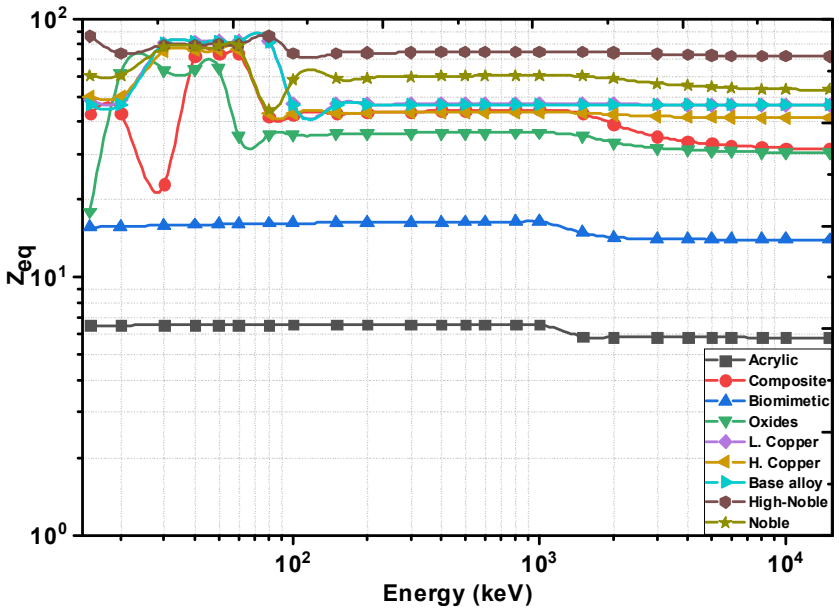

Fig 11. The variation of the equivalent atomic number [Zeq] with the photon energy for the selected dental samples.

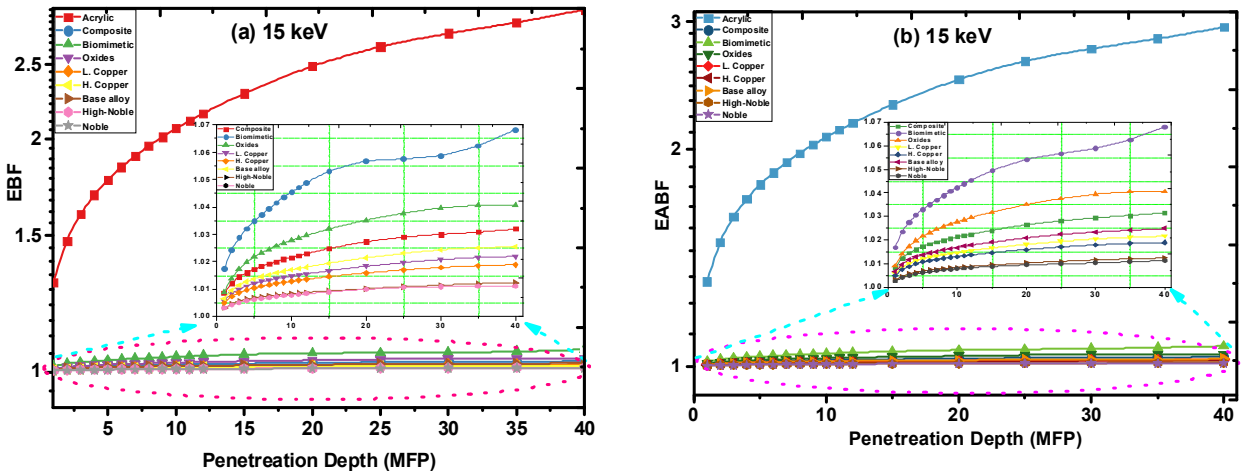

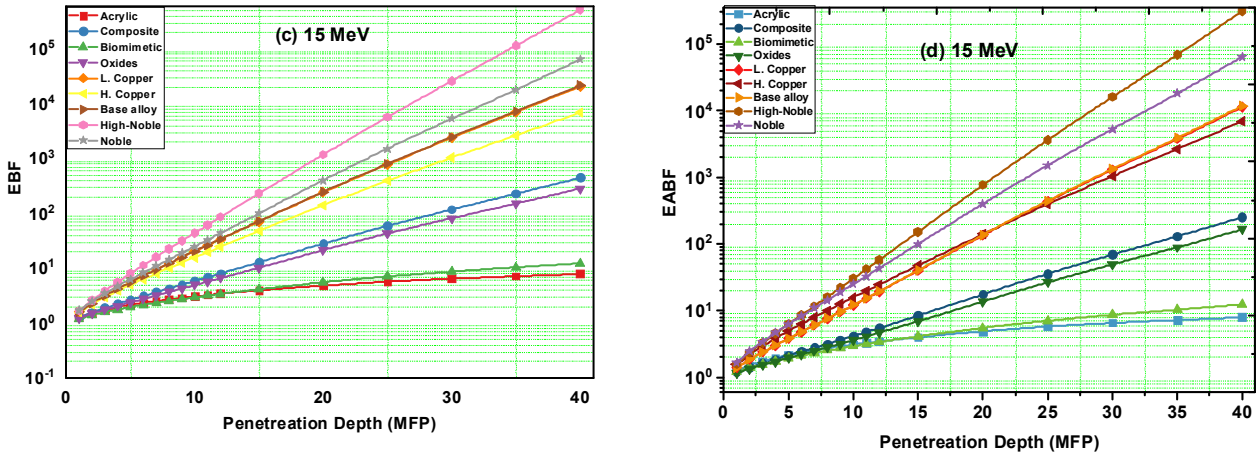

Figs 12 (a - d). Computed values of EBF and EABF for the tested samples at fixed incident photon energies 0.015 MeV and 0.15 MeV up to 40 MFP.

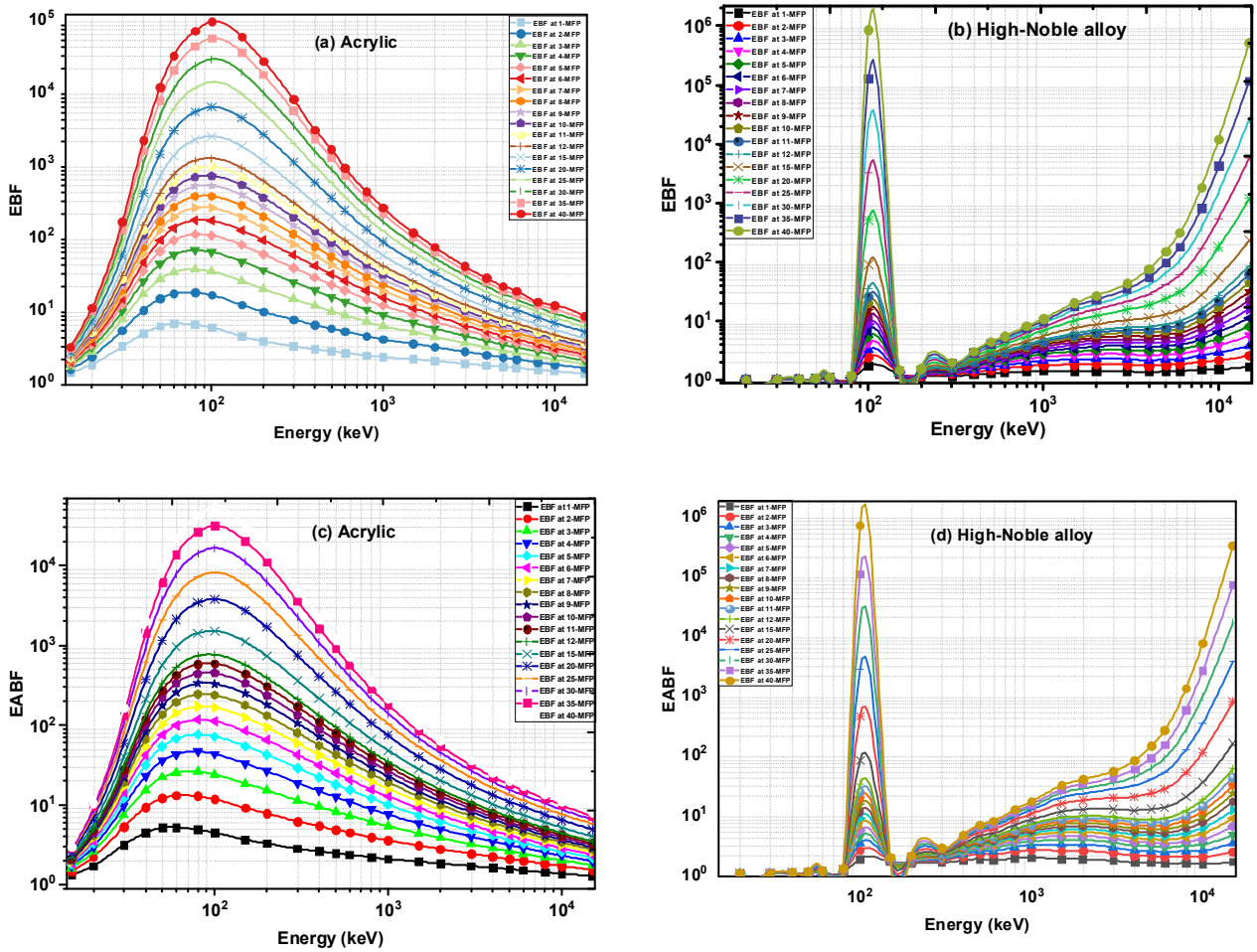

Figs 13. Variations of (a-b) EBF, and (c-d) EABF of acrylic (worst sample) and high-noble alloy (best sample), respectively, as a function of incident photon energy at different penetration depths.

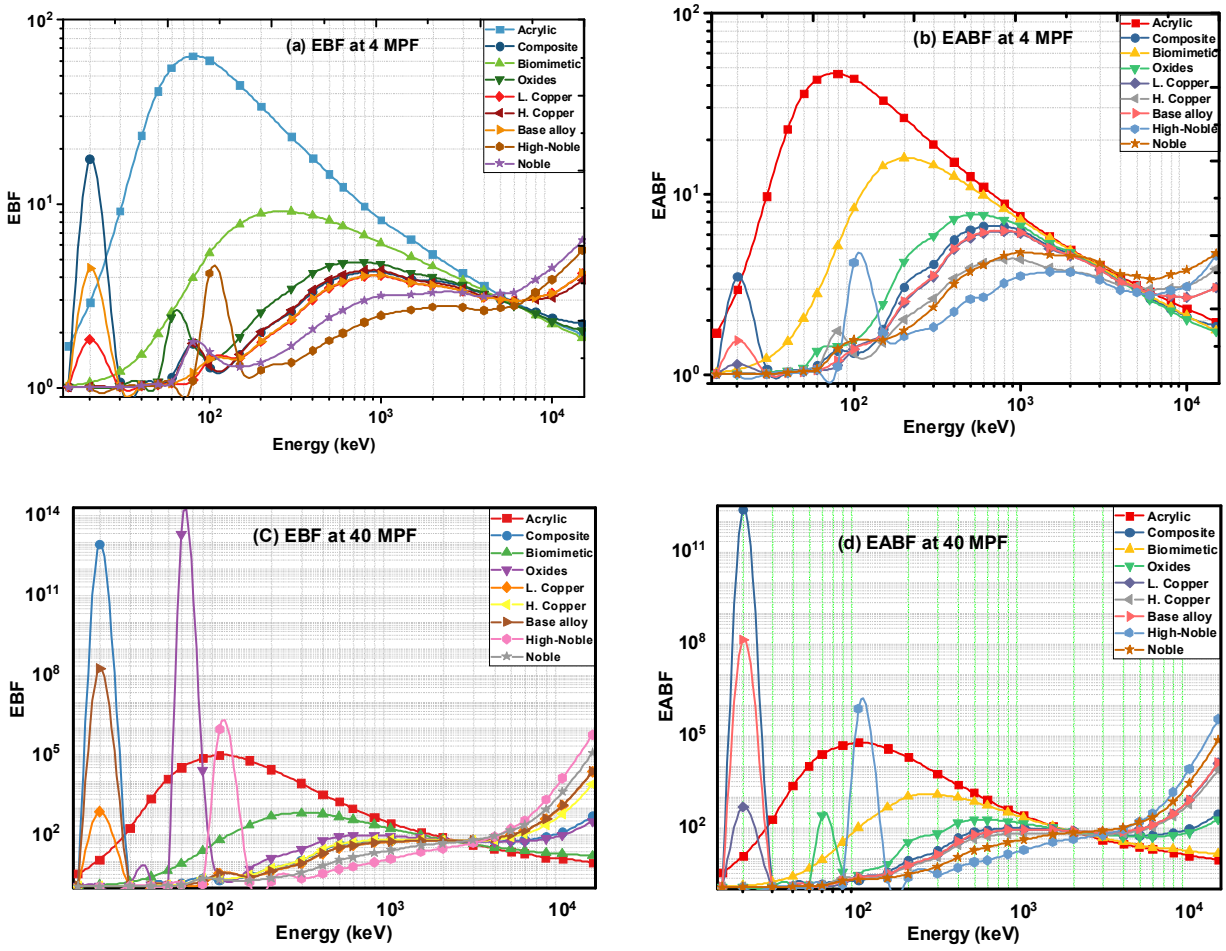

Figs 14. Variations of EBF and EABF as a function of incident photon energy at (a-b) 4 MFP and (c-d) 40 MFP penetration depth.

Table 4. Equivalent atomic number [Zeq] and G-P exposure [EBF] and absorption [EABF] buildup factor coefficients for acrylic and high-noble alloy samples.

Acrylic sample												
Energy [keV]	R	Z_{eq}	EBF					EABF				
			a	b	c	d	X_k	a	b	c	d	X_k
15	0.168	6.512	0.159	1.305	0.505	-0.079	14.289	0.158	1.312	0.504	-0.078	14.500
20	0.349	6.526	0.107	1.695	0.652	-0.052	15.715	0.108	1.714	0.651	-0.053	15.610
30	0.674	6.532	0.017	3.020	0.981	-0.018	14.414	0.017	3.166	0.982	-0.017	14.489
40	0.842	6.535	-0.087	4.532	1.487	0.036	13.727	-0.085	4.468	1.479	0.034	13.934
50	0.916	6.537	-0.138	5.778	1.848	0.060	14.067	-0.135	5.204	1.823	0.057	14.191
60	0.952	6.541	-0.173	6.257	2.133	0.079	14.054	-0.166	5.267	2.081	0.073	14.161

80	0.980	6.548	-0.208	6.009	2.460	0.094	13.793	-0.194	4.891	2.339	0.083	14.027
100	0.990	6.552	-0.212	5.501	2.531	0.092	14.394	-0.194	4.508	2.377	0.080	14.652
150	0.997	6.554	-0.225	4.146	2.630	0.100	14.123	-0.196	3.652	2.381	0.078	14.645
200	0.999	6.558	-0.219	3.545	2.531	0.096	14.066	-0.186	3.284	2.267	0.076	14.787
300	1.000	6.563	-0.193	3.039	2.255	0.083	14.206	-0.171	2.823	2.087	0.068	14.524
400	1.000	6.565	-0.175	2.760	2.068	0.074	13.809	-0.152	2.624	1.909	0.061	14.472
500	1.000	6.566	-0.156	2.587	1.908	0.069	14.155	-0.138	2.460	1.792	0.058	14.922
600	1.000	6.566	-0.141	2.463	1.784	0.059	13.898	-0.122	2.378	1.673	0.048	14.547
800	1.000	6.566	-0.121	2.270	1.626	0.055	13.934	-0.107	2.200	1.552	0.045	14.154
1000	1.000	6.568	-0.102	2.152	1.503	0.047	13.892	-0.089	2.099	1.442	0.038	14.505
1500	0.998	5.890	-0.070	2.018	1.317	0.035	13.699	-0.060	1.940	1.276	0.027	14.296
2000	0.993	5.864	-0.045	1.905	1.195	0.022	14.046	-0.038	1.842	1.169	0.015	14.480
3000	0.975	5.857	-0.015	1.756	1.059	0.007	12.081	-0.011	1.715	1.051	0.003	14.307
4000	0.951	5.853	0.004	1.657	0.985	-0.008	24.485	0.003	1.627	0.989	-0.002	13.110
5000	0.924	5.853	0.017	1.578	0.938	-0.011	14.561	0.014	1.565	0.946	-0.007	14.884
6000	0.897	5.851	0.026	1.527	0.907	-0.015	14.437	0.030	1.520	0.900	-0.018	12.463
8000	0.842	5.849	0.038	1.441	0.869	-0.033	16.671	0.034	1.433	0.880	-0.017	11.976
10000	0.789	5.847	0.042	1.374	0.855	-0.020	12.503	0.040	1.380	0.859	-0.022	14.347
15000	0.675	5.846	0.046	1.277	0.839	-0.029	15.089	0.047	1.285	0.837	-0.032	15.645
high-noble alloy												
Energy [keV]	R	Z_{eq}	EBF					EABF				
			a	b	c	d	X_k	a	b	c	d	X_k
15	0.001	85.96	-	-	-	-	-	-	-	-	-	-
20	0.001	73.68	0.139	1.003	0.466	-0.082	24.935	0.139	1.003	0.466	-0.081	24.858
30	0.003	79.46	0.228	1.008	0.342	-0.097	15.342	0.251	1.008	0.324	-0.112	13.270

40	0.008	79.59	0.247	1.015	0.318	-0.091	14.643	0.259	1.015	0.309	-0.099	13.634
50	0.014	79.72	0.255	1.026	0.308	-0.102	14.112	0.266	1.027	0.295	-0.107	14.257
60	0.024	79.69	0.259	1.037	0.318	-0.119	13.976	0.273	1.041	0.296	-0.121	13.905
80	0.040	86.00	0.234	1.050	0.360	-0.114	13.893	0.299	1.066	0.274	-0.144	13.736
100	0.025	73.54	0.153	1.758	0.840	-0.128	16.029	0.160	1.784	0.810	-0.130	16.427
150	0.066	73.93	0.354	1.253	0.145	-0.086	15.112	0.315	1.593	0.107	-0.020	24.194
200	0.125	74.13	0.348	1.156	0.246	-0.196	13.688	0.629	1.522	0.074	-0.298	14.010
300	0.272	74.36	0.170	1.169	0.484	-0.082	13.614	0.400	1.558	0.200	-0.220	13.309
400	0.414	74.49	0.124	1.231	0.598	-0.065	14.143	0.297	1.673	0.322	-0.187	13.703
500	0.529	74.57	0.099	1.289	0.669	-0.053	14.135	0.238	1.784	0.413	-0.155	13.735
600	0.615	74.66	0.081	1.332	0.719	-0.044	13.698	0.167	1.701	0.533	-0.106	13.577
800	0.727	74.74	0.058	1.395	0.793	-0.033	13.708	0.130	1.820	0.621	-0.086	13.575
1000	0.793	74.71	0.043	1.430	0.849	-0.028	13.371	0.107	1.860	0.687	-0.077	13.528
1500	0.845	74.60	0.014	1.417	0.974	-0.021	14.328	0.060	1.779	0.837	-0.057	13.861
2000	0.809	74.23	0.007	1.427	1.011	-0.020	13.403	0.066	1.763	0.840	-0.069	13.442
3000	0.692	73.42	0.014	1.410	1.023	-0.039	13.411	0.087	1.666	0.812	-0.104	13.539
4000	0.584	72.81	0.020	1.375	1.031	-0.045	13.722	0.100	1.554	0.799	-0.118	13.852
5000	0.497	72.44	0.051	1.414	0.957	-0.074	13.946	0.126	1.548	0.752	-0.143	14.141
6000	0.428	72.23	0.058	1.425	0.955	-0.079	14.310	0.132	1.509	0.755	-0.148	14.292
8000	0.331	71.96	0.064	1.515	0.985	-0.085	14.146	0.126	1.514	0.805	-0.146	14.304
10000	0.265	71.85	0.031	1.539	1.146	-0.057	14.072	0.086	1.463	0.961	-0.110	14.196
15000	0.174	71.65	0.014	1.680	1.340	-0.047	13.624	0.048	1.598	1.195	-0.083	13.843

CONCLUSIONS

Radiological characterization of dental materials has been sparsely addressed in the literature. This study expands that scope by evaluating the essential attenuation properties of widely used dental restorative materials. The findings provide useful reference data for future radiation-interaction and dosimetric research in dental applications. The main conclusions are summarized as follows:

a. The H-Noble, Noble, and Base alloys sample have the highest μ and μ_m with the lowest HVL, TVL, and MFP values.
b. The cross-sections areas; σ_a and σ_e, and hence Z_{eff} are highest for H-Noble alloy and lowest for Acrylic sample in the given photon energy range.
c. In the lower photon energy regions, many variations in shielding characteristics were observed due to different X-ray absorption-edges of constituent high-Z elements.
d. Lowest EBF and EABF were also observed for H-Noble, Noble and Base alloys in intermediate [0.1–5 MeV] energy region and Zirconium in higher [5–15 MeV] energy region.

REFERENCES

1) B. Oto, N. Yıldız, T. Korkut, and E. Kavaz, Nucl. Eng. Des. 293 (2015) 166.
2) H. Gökçe, O. Güngör, and H. Yılmaz, Radiat. Phys. Chem. 185 (2021) 109519.
3) W. Chaiphaksa et al., N. Mater. Today Proc. 65 (2022) 2416.
4) M. Sayyed et al., J. Non-Cryst. Solids 507 (2019) 30.
5) Mostafa, S.A. Issa, and M. Sayyed, J. Alloys Compd. 708 (2017) 294.
6) M. Kamislioglu, J. Mater. Sci. Mater. Electron. 32 (2021) 12690.
7) O. Olarinoye and C. OcheIran. J. Med. Phys. 18 (2021) 139.
8) M. Al-Buriahi et al. Optik 257 (2022) 168821.
9) B. Alım et al. Radiat. Phys. Chem. 166 (2020) 108455.
10) S. Yin et al. Crystals 12 (2022) 178.
11) X. Zhang et al. Mater. Des. 205 (2021) 109722.
12) B. Oto et al. Ceram. Int. 45 (2019) 23681.
13) M. Sayyed et al. Radiat. Phys. Chem. 200 (2022) 110096.
14) Y. Slimani et al. J. Mater. Sci., Mater. Electron. 32 (2021) 20867.
15) M. Mhareb et al. Ceram. Int. 46 (2020) 28877.
16) A.M. Osman, ASME. ASME J of Nuclear Rad Sci. 9 (2023) 1.
17) B. Körpınar et al. Prog. Nucl. Energy 126 (2020) 103424.
18) T. Bel, C. Arslan, and N. Baydogan, Mater. Chem. Phys. 221 (2019) 58.
19) A.M. Osman, J Nucl Ene Sci Power Generat Technol 8 (2019) 2.
20) M. Sayyed et al. Materials 14 (2021) 3772.
21) D.S. Baykal, H.O. Tekin, R.B.C., and Mutlu, Int. J. Comput. Exp. Sci. Eng. 7 (2021) 99.

22) A.M. Osman et al. Annals of Nuclear Energy 78 (2015) 146.

23) A.M. Abdelmonem, A.M. Osman, and A.M. Ali, Radiation Effects and Defects in Soli 179 (2024) 1.

24) H. Yayka et al. J. Mater. Sci., Mater. Electron. 33 (2022) 2350.

25) J.S. Alzahrani et al. Radiat. Phys. Chem. 195 (2022) 110090.

26) F. Akman et al. J. Alloy. Comp. 772 (2019) 516.

27) M.K. Hamad, Ann. Nucl. Energy 184 (2023) 109687.

28) A.M. Osman, Int. J. Adv. Nucl. React. Des. Technol. 5 (2023) 1.

29) F.C. Hila et al. Radiation Physics and Chemistry 182 (2021) 1.

30) L. Gerward et al. Radiat. Phys. Chem. 60 (2001) 23.

31) R.G. Craig and J.M. Powers, Restorative Dental Materials, 13th ed., Mosby, St. Louis (2012) 207.

32) E. Sakar et al. Radiat. Phys. Chem. 166 (2020) 108496.

33) N. Sabry et al. Radiat. Phys. Chem. 193 (2022) 109989.

34) F. Daphne and D.J. Jackson, Hawkes Physics Reports 70 (1981) 169.

35) H. Sahadath et al. Radioprotection 50 (2015) 203.

36) T. Kaur, J. Sharma, and T. Singh, Int J. Pure Appl. Phys 13 (2017) 222.

37) M.J. Kamislioglu, Mater. Sci. Mater. Electron. 32 (2021) 12690.

38) Y. Harima, Nucl. Sci. Eng. 83 (1983) 299.

39) American National Standard [ANS], (1991). ANSI/ANS 6.4.3.

40) P. Tamayo et al. Construction and Building Materials 319 (2022) 126098.

41) Basanta Subedi, Jeevan Paudel, and Tika Ram Lamichhane, Heliyon 9 (2023) 17725.

42) Y. Aboudeif et al. J. Instrum. 15 (2020) 08005.

43) H.O. Tekin et al. Open Chem. 20 (2022) 69.